Effects of 1-GeV uranium ion irradiation on vortex pinning in single crystals of the high-temperature superconductor $YBa_2Cu_3O_{7-\delta}$

L. M. Paulius
Materials Science Division and Science and Technology Center for Superconductivity, Argonne National Laboratory, Argonne, Illinois 60439
and Department of Physics, Western Michigan University, Kalamazoo, Michigan 49008

J. A. Fendrich,* W.-K. Kwok, A. E. Koshelev, V. M. Vinokur, and G. W. Crabtree
Materials Science Division and Science and Technology Center for Superconductivity, Argonne National Laboratory, Argonne, Illinois 60439

B. G. Glagola
Physics Division, Argonne National Laboratory, Argonne, Illinois 60439
(Received 12 February 1997)

We report magnetoresistance measurements of the effects of 1-GeV uranium ion irradiation on a clean, untwinned single crystal of $YBa_2Cu_3O_{7-\delta}$. In order to isolate the effects of irradiation, we masked one region of the crystal from the radiation so that it would retain its original characteristics. The columnar defects created by the irradiation dramatically alter the shape of the irreversibility line. In addition, the pinning anisotropy of the vortices is reversed by the irradiation. We estimate the pinning energy from the depinning angle and compare it to the pinning energy measured in twinned single crystals. We show that the onset of pinning from the columnar defects occurs very close to the zero-field superconducting transition temperature, well into the vortex liquid state. In addition, measurements across the boundary between the irradiated and unirradiated regions directly demonstrate that the dissipative behavior of vortex flow due to the Lorentz force is similar to the dissipation of two resistors in series for this geometry. [S0163-1829(97)00925-9]

I. INTRODUCTION

The magnetic phase diagrams of the high-temperature superconductors contain a rich assortment of phases whose properties depend on the number and type of defects present in the material. A large portion of the phase diagram is occupied by the vortex liquid state created by the high thermal energies, small superconducting coherence lengths, and large anisotropies of these materials. In crystals which are relatively free of defects, a first-order phase transition from a vortex liquid state to a vortex solid state has recently been reported in both $Bi_2Sr_2CaCu_2O_8$ (Refs. 1–4) and $YBa_2Cu_3O_{7-\delta}$.[5–11] In the presence of defects, it has been shown that the first-order transition is suppressed,[12] consistent with theoretical predictions of a continuous phase transition to a glassy solid whose character depends on the number and dimensionality of the defects.[13–19] A vortex glass has been predicted to occur in the presence of weak random point defects[20] such as oxygen vacancies and atomic scale defects, while a Bose glass state has been predicted[21,22] for correlated defects like twin boundaries and the amorphous columnar tracks induced by heavy ion irradiation.

In addition to the wealth of fundamental scientific information vortex studies can yield, there is also strong technological interest, since the commercial applicability of these high-temperature superconductors relies heavily on their ability to carry high currents, which, in turn, is determined by the effectiveness of the pinning sites in these materials.

The columnar defects created by heavy ion irradiation are among the most effective pinning sites in high-temperature superconductors. These defects enhance the critical current and shift the irreversibility line to higher temperatures, thereby reducing the range of the vortex liquid state and making these materials more amenable for widespread technological applications.[23–35]

Several experimental studies have addressed the microscopic pinning behavior of the columnar defects induced by heavy ion irradiation.[16,30,36–43] However, in many cases, these studies were conducted on thin films and twinned crystals, samples which contain a large number of pre-existing correlated defects. Furthermore, even among twin-free samples, one must also consider the role of oxygen vacancies which could lead to large numbers of pre-existing point defects. In order to isolate the effects of the induced columnar defects, it is important to begin with a clean, well characterized crystal. Since the first-order melting transition is very sensitive to the presence of defects, the occurrence of the melting transition is a strong indication of crystal quality.

In this study, we present the results of 1-GeV uranium ion irradiation on a clean untwinned $YBa_2Cu_3O_{7-\delta}$ single crystal. This crystal displays a clear first-order vortex solid to liquid melting transition. We use a unique geometry to irradiate the sample: one region of the crystal was masked with a tantalum foil while the remainder of the crystal was exposed to the heavy ions. A similar masking technique was recently used by Harada *et al.*,[44] where they performed Lorentz microscopy experiments on a $Bi_2Sr_{1.8}CaCu_2O_x$ single crystal irradiated with Au. This allows us to study the effect of the columnar defects on vortex pinning and compare directly with the unirradiated region of the *same* crystal. In addition, the dissipation across a mixed region containing both areas can be studied.

We performed electrical transport measurements in magnetic fields up to 8 T. We report on the effects of heavy ion

irradiation on the superconducting properties including the transition temperature, the current-voltage characteristics, the irreversibility line, and the angular dependence of the pinning. We determine the pinning energy per unit length and compare the values with results on twinned single crystals.

II. EXPERIMENTAL SETUP

The crystals were grown by a self-flux method using powders of Y_2O_3, $BaCO_3$, and CuO with a purity of 99.99% or better as described elsewhere.[45] The crystals were subsequently annealed for 10 days in flowing oxygen at 430 °C. This method yields platelet-shaped single crystals with the crystallographic *c* axis perpendicular to the face of the platelet.

An untwinned and two twinned $YBa_2Cu_3O_{7-\delta}$ single crystals were used in our study. The untwinned single crystal used in our investigation was obtained by detwinning the crystal under flowing oxygen at 420 °C while applying uniaxial pressure in the *ab* plane of the crystal. This crystal was a thin platelet with dimensions of $0.35(w)\times1.41(l)\times0.02(t)$ mm^3. The electrical contacts were made to the crystal in the standard four-probe configuration. We attached gold wires with silver epoxy which was cured in flowing oxygen for 6 h at 420 °C.

For the heavy ion irradiation, part of the crystal was covered with a tantalum mask and the other region was irradiated with $^{238}U^{40+}$ ions at ATLAS (Argonne Tandem Linear Accelerator System) with the ion beam directed parallel to the *c* axis of the crystal. The crystal was irradiated at room temperature with a beam current of 1 enA and an ion energy of 1 GeV. The Monte Carlo simulation program TRansport of Ions in Matter[46] (TRIM) gives the range of these ions in $YBa_2Cu_3O_7$ as 28.4 μm, which is greater than the 20 μm thickness of the crystal, ensuring that the ions traverse the entire thickness of the crystal. The total irradiation dose was 1×10^{11} ions/cm^2. At this dose, the number of vortices equals the number of ion tracks in an applied magnetic field of 2 T. This field is referred to as the matching field B_ϕ. Multiple electrical contacts were made on the crystal, two on the ends for passing the current in the *ab* plane of the crystal, and four contacts for measuring the voltage in various regions of the crystal as shown in Fig. 1.

Two twinned single crystals were measured to provide a comparison of the pinning effects of twin boundaries with the defects caused by U ion irradiation. These twinned crystals, with dimensions on the order of $\sim0.8(l)\times0.4(w)\times0.05(t)$ mm^3, were cleaved from a larger piece to obtain a single family of twin boundaries oriented parallel to the long axis of the crystal. Current contacts were attached so that the current flowed parallel to the *ab* plane and parallel to the twin boundaries as shown in Fig. 2. This geometry induces a Lorentz force perpendicular to the twin boundaries when the field is parallel to the *c* axis. In this configuration, the vortices experience the maximum pinning effect from the twin boundaries. [For a more complete study of the pinning properties of twin boundaries, see Fleshler *et al.* (Ref. 47).]

The resistivity was measured as a function of both temperature and field using a standard four-probe technique with low frequency (17 Hz) ac currents. The current density ranged from 0.7 to 28 A/cm^2 and was directed parallel to the *ab* plane of the crystal. Current-voltage characteristics were determined with a dc current source and a nanovoltmeter.

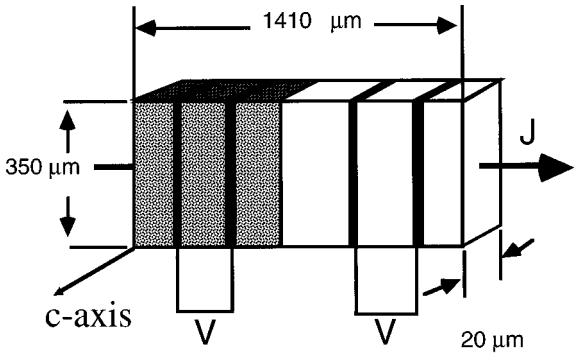

FIG. 1. Schematic drawing of the untwinned crystal used to study the effects of U ion irradiation. One region of the crystal was irradiated with 1 GeV U ions and the ion beam was parallel to the *c* axis of the crystal. The current flowed in the *ab* plane of the crystal and the voltage could be monitored in either the irradiated, unirradiated, or across both regions of the crystal.

Measurements in an applied magnetic field were performed by placing the crystal in the bore of two orthogonal superconducting magnets, an 8 T longitudinal magnet and a 1.5 T split-coil transverse magnet. The crystal was oriented with the *c* axis of the crystal parallel to the longitudinal magnet and the net field was always directed perpendicular to the current. For $H\leqslant1.5$ T, the net magnetic field could be rotated from $+90°$ to $-90°$ relative to the *c* axis of the crystal simply by varying the relative magnitude of the two orthogonal fields. This technique can yield an angular resolution of 0.005°.[48] For fields $H>1.5$ T, the physical orientation of the crystal must be changed in order to probe the full angular range.

III. RESULTS

A. Transition temperatures

Figure 3 shows the normalized resistivity and its derivative as a function of temperature for the unirradiated and the irradiated regions of the untwinned crystal in zero applied

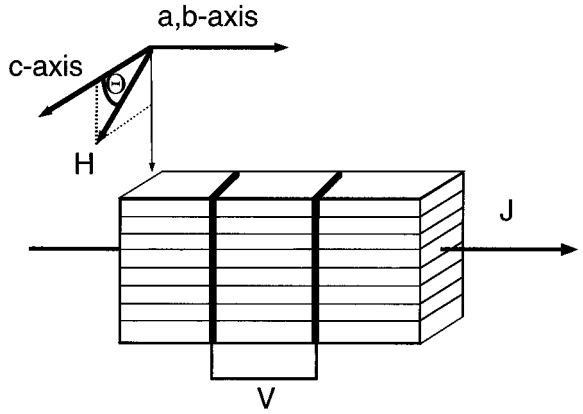

FIG. 2. Schematic drawing of the twinned crystals. The current flowed parallel to the twin boundaries and in the *ab* plane of the crystals. The applied magnetic field was always oriented perpendicular to the current.

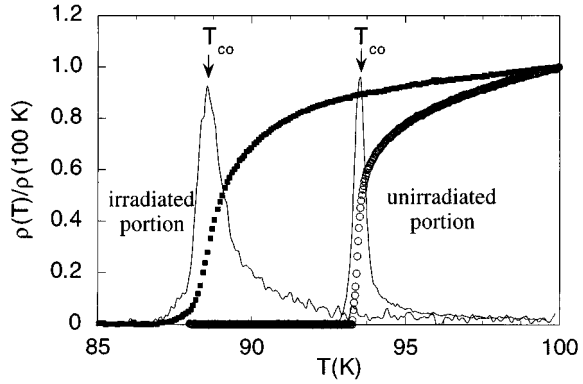

FIG. 3. Normalized resistivity and its derivative as a function of temperature for both the unirradiated and irradiated regions of the crystal. Open circles and the solid squares represent the data for the unirradiated and irradiated regions of the crystal, respectively. The temperature derivatives are shown by the solid lines. The arrows indicate the values of T_{c0} for each region of the crystal.

magnetic field. We define T_{c0} as the peak in the temperature derivative of the resistivity $d\rho(T)/dT$ for the zero-field transition. The transition width ΔT_{c0} is taken as the difference between the temperatures at which the resistivity drops from 90 to 10% of the extrapolated normal-state values. The unirradiated region of the crystal has a superconducting transition temperature T_{c0} of 93.5 K and a sharp transition, $\Delta T_{c0}<400$ mK. In the irradiated region, T_{c0} dropped by ~ 5 K to 88.5 K and the transition width increased by roughly a factor of 5 to $\Delta T_{c0}\approx 2.1$ K. This drop in T_{c0} is larger than is typically reported for other, less massive, ion irradiations.[26,27,49] The normal-state resistivity was also dramatically affected by the irradiation, with the resistivity increasing about an order of magnitude after irradiation. For comparison, Bourgault *et al.*[26] measured the effects of 3.5 GeV Xe ion irradiation on polycrystalline samples of $YBa_2Cu_3O_{7-\delta}$ for fluences ranging from 0 to $\sim 9\times 10^{12}$ ions/cm^2. They see an order of magnitude increase in the normal-state resistivity for a fluence of $\sim 3\times 10^{12}$ ions/cm^2 and a drop of 5 K in T_c for a fluence of $\sim 5\times 10^{12}$ ions/cm^2. These doses are much larger than the 1×10^{11} ions/cm^2 dose that our sample received.

We performed linear fits to the normal-state resistivity. The extrapolated zero-temperature resistivity shows a change from a small negative intercept in the unirradiated region of the sample to a large positive intercept in the irradiated region. In addition, the slope of the resistivity $d\rho/dT$ increases by approximately a factor of 7 after the irradiation. These changes indicate the presence of extensive damage throughout the bulk of the crystal from the irradiation.

B. Magnetic-field dependence of the resistive transition

1. Unirradiated region

The resistive transition broadens in the presence of an applied magnetic field and the zero resistance point shifts to lower temperatures with increasing field. This is shown for the unirradiated region in Figs. 4(a) and 4(b) for the magnetic field applied parallel to the c axis and the ab plane, respectively, with a current density of $J=0.7$ A/cm^2. The

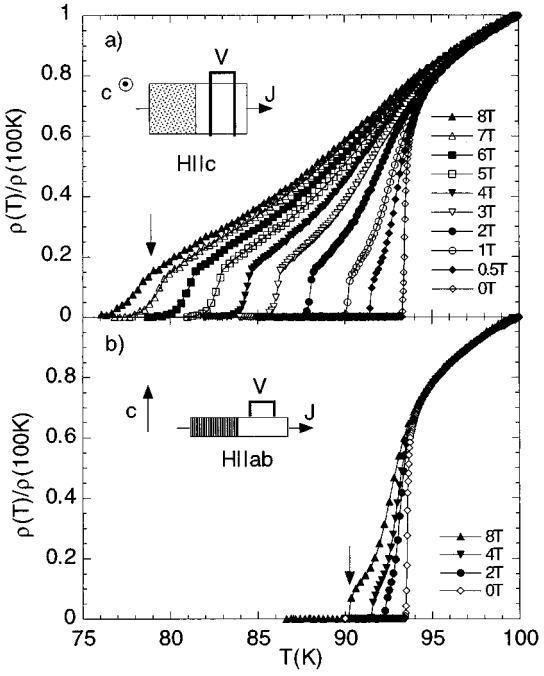

FIG. 4. Normalized electrical resistivity of the unirradiated region of the crystal as a function of temperature for magnetic fields applied (a) parallel to the c axis and (b) parallel to the ab plane of the crystal. The current flowed in the ab plane and the fields ranged from 0 to 8 T. In each case, the field was perpendicular to the current. The solid lines are a guide to the eye and the arrows in both figures indicate the kink in the curve for $H=8$ T.

plot shows the normalized resistivity $\rho/\rho(T=100\text{ K})$ as a function of temperature for applied magnetic fields $0T\leqslant H\leqslant 8$ T. The transitions become broader and ''fan-shaped'' with increasing magnetic field. This broadening of the transition above $\rho>0.5\rho_n$ is usually attributed to thermodynamic fluctuations of the order parameter.[50,51] In high-T_c materials, the effects of fluctuations are greatly enhanced because of the short coherence lengths, the large anisotropies, and the high values of T_c. The Ginzburg number G_i is a measure of the importance of thermal fluctuations and is related to the temperature region ΔT over which thermal fluctuations play a role by $\Delta T/T_c\approx G_i$. The Ginzburg number is given by $G_i=1/2(\gamma T_c/H_c^2\xi^3)^2$ and $G_i(H)\approx G_i^{1/3}(H/H_{c2})^{2/3}$,[52] where H_c is the thermodynamic critical field, γ is the anisotropy parameter ($\gamma^2=m_c/m_{ab}>1$), where m_c and m_{ab} are the effective mass along the c axis and ab plane, respectively, ξ is the coherence length, and H_{c2} is the upper critical field. In conventional low-temperature superconductors, G_i is very small, on the order of 10^{-7}. However, in $YBa_2Cu_3O_{7-\delta}$, G_i is much larger, $G_i\approx 10^{-2}$.[53]

Due to the anisotropy of the material, the broadening of the transition is more severe when the magnetic field is applied parallel to the c axis than when it is applied parallel to the ab plane. This can be seen if we look at the temperature range T_W over which the reduced resistivity drops from 0.5 to 0.1. For $H\|ab$ T_W increases by a factor of 11 when the field is increases from 0 to 8 T [$T_W(0\text{ T})\approx 0.2$ K and $T_W(8\text{ T})\approx 2.2$ K], but for $H\|c$ T_W increases a factor of 50 over the same field range [$T_W(0\text{ T})\approx 0.2$ K and $T_W(8\text{ T})\approx 10$ K].

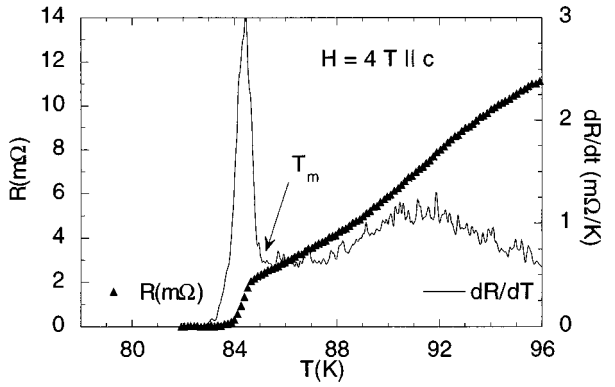

FIG. 5. Electrical resistance and its derivative as a function of temperature for the unirradiated region of the crystal in a magnetic field of 4 T applied parallel to the c axis of the crystal. The arrow shows the vortex melting temperature T_m.

The resistivity in applied magnetic fields shows a smooth decrease at higher temperatures followed by an abrupt kink at lower temperatures where the resistivity drops very sharply to zero. (The kink in the resistivity is indicated by arrows in Fig. 4 for the transition in an 8 T applied field.) This kink occurs for both directions of the applied field, $H\|ab$ and $H\|c$. The current-voltage characteristics of the crystal are very different for temperatures above and below the kink. Above the kink, the behavior is Ohmic (i.e., the voltage is a linear function of the current) whereas below the kink, the behavior is highly non-Ohmic. This kink in the resistive transition is associated with a first-order melting transition of the vortex solid to a vortex liquid.[5–7,9,10] Recent results by Fendrich *et al.*[8] on simultaneous measurements of both magnetization and resistivity show that the kink in the resistive transition occurs at the same temperature and field as a jump in the magnetization. The jump in the magnetization corresponds to a change in the vortex density on melting, a clear indication of a first-order transition. In Fig. 5 we show both the electrical resistance and its derivative as a function of temperature in a 4 T magnetic field applied parallel to the c axis. Magnetic measurements[8] indicate that the onset of the melting transition occurs at the temperature where $d\rho/dT$ first begins its sharp upturn, as indicated by the arrow in the figure.

For fields applied parallel to the c axis of the crystal, the kink in the resistivity becomes noticeably less sharp as the field is increased above 6 T. Safar *et al.*[54] have presented data on a clean untwinned single crystal of $YBa_2Cu_3O_{7-\delta}$ which suggest that for $H\|c$, the first-order melting transition at low fields gives way to a continuous or second-order phase transition at high fields. They find that this crossover occurs at a well defined value of the magnetic field H_{cr} ($H_{cr}\approx 10$ T in their crystal). They propose the existence of a critical point in the H-T phase diagram, above which the first-order phase transition does not occur. The smearing out of the kink in our data for $H\|c$ at high fields is consistent with their interpretation, though H_{cr} appears to be lower in our crystal. However, it is interesting to note that for $H\|ab$, the kink still remains sharp for fields up to 8 T, indicating that the critical point may occur at much higher fields for this orientation.

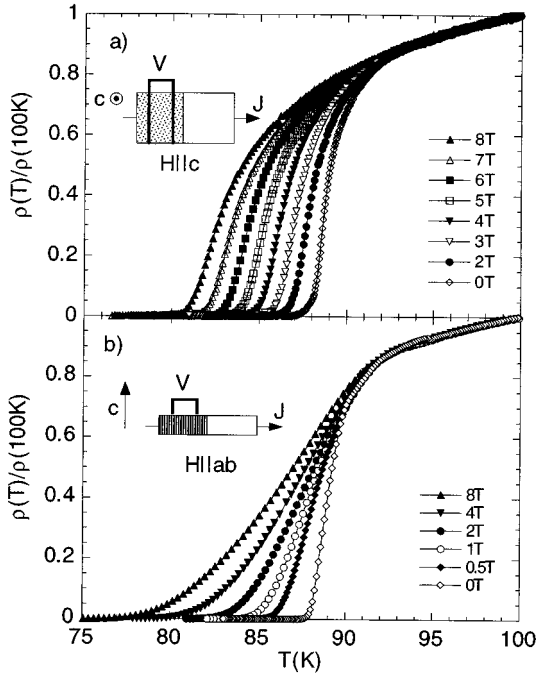

FIG. 6. Normalized electrical resistivity of the irradiated region of the crystal as a function of temperature for magnetic fields applied (a) parallel to the c axis and (b) parallel to the ab plane of the crystal. The current flowed in the ab plane and the fields ranged from 0 to 8 T. In each case the field was perpendicular to the current. The solid lines are a guide to the eye.

2. Irradiated region

The resistive transition in magnetic fields is dramatically altered after irradiation with U ions. This can be seen in Fig. 6 which shows the temperature dependence of the resistivity in the irradiated region of the crystal for $H\|c$ (a) and $H\|ab$ (b) for fields ranging from 0 to 8 T with a current density of $J=0.7$ A/cm^2. As discussed previously, the zero-field transition temperature is shifted down to 88.5 K, a drop of 5 K compared to the unirradiated region of the crystal.

The resistive transitions in the irradiated region of the crystal do not display the kink associated with the vortex melting transition. The resistivity drops smoothly to zero, both for the field parallel to the c axis and to the ab plane. Another striking difference is that after irradiation, the anisotropy in the resistivity is reversed. In the unirradiated region, the resistive transitions were much broader for $H\|c$ than for $H\|ab$ due to the inherent anisotropy of the relatively clean crystal. In contrast, in the irradiated region the resistive transitions are much broader when $H\|ab$ than for $H\|c$ (and $\|$ ion tracks). For $H\|ab$, the ''fan-shaped'' broadening of the transitions in increasing field are even more pronounced than in the unirradiated region of the crystal. However, for $H\|c$, the transitions are no longer ''fan-shaped'' and the slopes of the transition are nearly parallel.

In the unirradiated region of the sample for $H\|c$, the transition width T_w increased from $T_w(0\text{ T})\approx 0.2$ K to $T_W(8\text{ T})\approx 10$ K but in the irradiated region T_w increases by less than a factor of 3 from $T_w(0\text{ T})\approx 1$ K to $T_w(8\text{ T})\approx 2.5$ K. For $H=8\text{ T}\|c$, the transition is roughly a factor of 4 broader in the unirradiated region of the crystal than in the irradiated section. In addition, the temperature at which the

resistivity drops to zero is shifted up from $T\sim 76$ K in the unirradiated region to $T\sim 80$ K in the irradiated region.

For $H\|ab$, the transition width in the unirradiated region increased from $T_w(0\ \mathrm{T})\approx 0.2$ K to $T_w(8\ \mathrm{T})\approx 2.2$ K and in the irradiated region it increases from $T_w(0\ \mathrm{K})\approx 1$ K to $T_w(8\ \mathrm{T})\approx 6$ K. Unlike the case for $H\|c$, the transition for $H=8\ \mathrm{T}\|ab$ is sharper in the unirradiated region than in the irradiated region (by nearly a factor of 4). This is a complete reversal in the anisotropy in the resistivity.

We were only able to perform measurements of the current-voltage characteristics down to $T/T_c\sim 0.97$ because of the limited sensitivity of our nanovoltmeter, and for current densities up to ~ 14 A/cm^2, limited by the heating from the contacts. Over this region, the current-voltage characteristics displayed Ohmic behavior in the irradiated portion of the crystal for $H\|c$.

The Bose glass theory predicts a temperature dependence of the resistivity which should scale as

$$\rho\propto(T-T_{\mathrm{BG}})^s, \tag{1}$$

where s is field independent and T_{BG} is the Bose glass transition temperature. While we do not find such a scaling behavior in the U ion irradiated sample, the resistivity for the twinned crystal could be described by Eq. (1) for $H\|c$. We found that s was field independent and equal to $\sim 5.2\pm 0.4$ for fields up to 7 T. Our results lie in the range of previously reported values, where s ranges from $s\approx 4$ (for $Tl_2Ba_2CaCu_2O_8$ thin films irradiated with Ag ions)[15] to $s\sim 6$ for both thin films and irradiated twinned crystals of $YBa_2Cu_3O_{7-\delta}$.[13,55]

C. Phase diagrams

1. Unirradiated region

The magnetic phase diagram for the unirradiated portion of the crystal is shown in Fig. 7(a) for both $H\|c$ and $H\|ab$. The melting line was determined from $d\rho/dT$ as shown in Fig. 5. The melting line is shifted to much higher temperatures when the orientation of the magnetic field is changed from $H\|c$ axis to $H\|ab$ plane. For both orientations of the field, the irreversibility lines can be fit to an equation of the form

$$H=H_0\left(1-\frac{T}{T_{c0}}\right)^{\alpha}, \tag{2}$$

where T_{c0} is the zero-field transition temperature, and H_0 and α are fitting parameters. These fits are shown as solid lines in Fig. 7(a).

As discussed by Blatter *et al.*,[52] the power-law fit given in Eq. (2) is a compact form for expressing the behavior of the melting line, where α is an ''effective'' exponent (for the implicit equation, see Houghton, Pelcouits, and Sudbo[56]). The form given in Eq. (2) is a convenient description of the melting line from which we can extract information about the anisotropy of the crystal. Our fits yielded values of $H_{0c}=77\pm 5$ T, $\alpha_c=1.23\pm 0.03$ for $H\|c$ and $H_{0ab}=611\pm 22$ T, $\alpha_{ab}=1.24\pm 0.04$ for $H\|ab$. For $H\|c$, previously reported results[7,54,57–59] lie in the range of $1.2\leqslant\alpha\leqslant 2$. For $H\|ab$ our fit value α_{ab} is consistent with previous reports by Kwok *et al.*[7] The ratio of H_{0ab}/H_{0c} yields the anisotropy ratio γ.

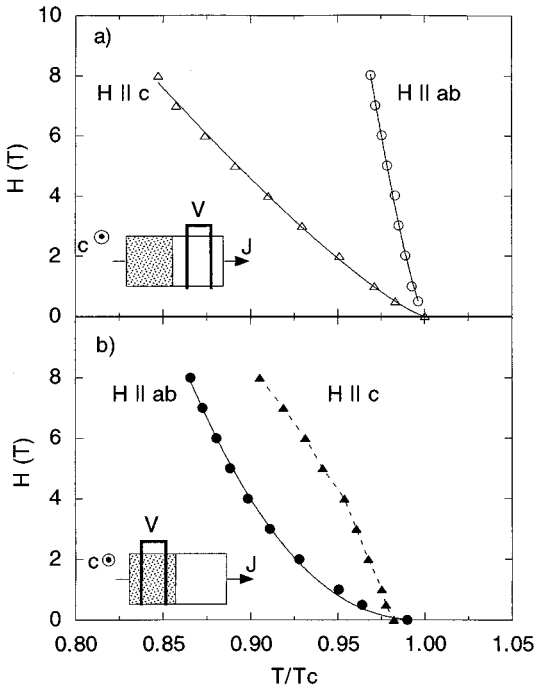

FIG. 7. (a) Irreversibility line as determined from the vortex melting temperature for the unirradiated region of the crystal for $H\|c$ (open triangles) and $H\|ab$ (open circles). The solid lines are fits to Eq. (2). (b) Irreversibility line for the irradiated region of the crystal for $H\|c$ (solid triangles) and $H\|ab$ (solid squares). Values were determined from resistivity measurements using a criterion of 1 $\mu\Omega$ cm to define T^*. The solid line is a fit to Eq. (2) and the dashed line is a guide to the eye.

Our results yield a value of $\gamma=7.6\pm 0.6$, which is in excellent agreement with the previous resistivity measurements of Kwok *et al.*[7] and is within the range of the values ($5\leqslant\gamma\leqslant 10$) obtained by other techniques.[60–65]

2. Irradiated region

In samples with correlated defects, the irreversibility line is marked by the Bose glass transition temperature T_{BG}, obtained from Eq. (1). In the irradiated region of the crystal, we cannot extract T_{BG} because we did not see the predicted scaling of the resistivity within the sensitivity of our experimental setup. However, we can qualitatively map out an irreversibility line by choosing a resistivity criterion of $\rho^*=1$ $\mu\Omega$ cm to define T^*. Since this is in the Ohmic region for the irradiated portion of the crystal, this criterion is independent of the current and gives an upper bound for the irreversibility line. Palstra *et al.* have argued such a resistivity criterion is more meaningful for determining the onset of J_c in high-T_c samples than a voltage criterion.[66] The absolute position of the irreversibility line lies slightly lower in temperature in the phase diagram than the nonzero resistivity criterion we use here. The results are shown in Fig. 7(b) for $H\|c$ and $H\|ab$. At very low fields ($H<0.2$ T), the irreversibility line for $H\|c$ lies below the line for $H\|ab$. However, as the field increases, the anisotropy of the irreversibility line reverses, with the irreversibility line for $H\|c$ shifted above the line for $H\|ab$. The irreversibility line for $H\|ab$ can be fit to Eq. (2), with values of $\alpha_{ab}=2.1\pm 0.1$ and $H_{0ab}=480\pm 82$ T. The ir-

reversibility line for $H\|c$ cannot be described by Eq. (2). The qualitative shape of the irreversibility line for $H\|c$ is changed from a positive curvature before irradiation to a negative curvature after irradiation. Similar behavior has also been observed in Au- (Ref. 16) and Pb- (Ref. 28) irradiated $YBa_2Cu_3O_7$ single crystals as well as Pb-irradiated $Bi_2Sr_2CaCu_2O_8$ and Tl-based superconductors.[67] It has been suggested[28] that the irreversibility line is determined by the temperature dependence of the strongest pinning centers in the sample. Thus the qualitative change in curvature may arise from the differences in the temperature dependence of the pinning of the pre- and post-irradiation defects in the crystal.

D. Angular dependence of the irreversibility line

Although theory predicts a similar scaling of the resistivity as $\rho(T)$ approaches zero for both the vortex glass (for point defects) and the Bose glass (for correlated defects), there is a pronounced difference in the angular dependence of the irreversibility temperature between the vortex glass and the Bose glass states. Due to the isotropic nature of point defects, the vortex glass theory predicts a smooth variation of the irreversibility line with angle, while the Bose glass theory predicts a sharp upward cusp in the irreversibility line as the angle between the field and the correlation direction approaches zero. This difference arises because the correlated volume near the vortex glass transition diverges isotropically, but in the Bose glass the correlations diverge with two different correlation lengths.[21]

This difference in the angular dependence of the irreversibility line can be seen clearly in Fig. 8 where we plot the reduced irreversibility temperature T^*/T_{c0} as a function of the angle Θ between the applied field and the c axis of the crystal. In Fig. 8(a) we plot T^*/T_{c0} for the unirradiated region of the crystal in an applied field of 0.5 T. The irreversibility line does not show any indication of a cusp near $\Theta=0°$. For comparison, we also show T^*/T_{c0} in applied fields of 1 and 4 T for a typical untwinned single crystal with a large number of point defects created by irradiation with 9 MeV protons to a fluence of 3×10^{16} p/cm^2.[68] In this sample, the irreversibility line decreases smoothly near $\Theta=0°$, which is consistent with the vortex glass theory.

In Fig. 8(b) we plot T^*/T_{c0}, as a function of angle for the U-irradiated region of the crystal in applied fields of 1 and 4 T with data on a twinned single crystal shown for comparison. Here, both samples have defects which are correlated along the c axis (i.e., along $\Theta=0°$) and both display the sharp ''cusp'' near $\Theta=0°$ which is associated with the Bose glass state.[21] We define the width of the cusp as half the angular distance between the minima in T^*. Neither the width of the cusp nor the qualitative shape of the cusp depended very strongly on our choice of resistivity criterion. There was no discernible change in the width when ρ^* was varied from 0.5 to 10 $\mu\Omega$ cm. The width of the cusp in the U ion irradiated sample decreases from $\sim70°$ to $\sim30°$ as the applied field is increased from 1 to 4 T. These results are comparable to the value of a cusp width of $\sim30°$ in a field of 3 T reported on a crystal irradiated with 1-GeV Xe ions at $\pm7.5°$ from the c axis creating splayed columnar defects with a total matching field of $B_\phi=2$ T. The width of the cusp is much broader for the U ion crystal than for the crystal with twin boundary defects ($\sim30°$ as opposed to $\sim9°$ in $H=4$ T), illustrating the strong pinning by the columnar defects created by the U ion irradiation.

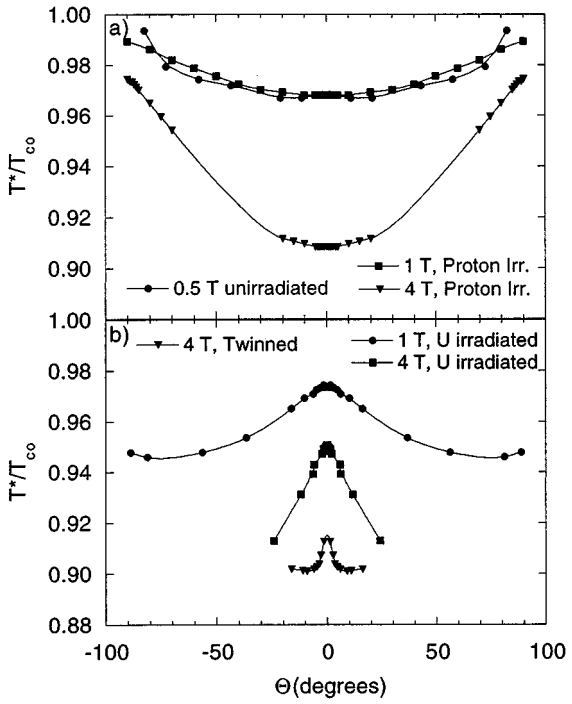

FIG. 8. T^*/T_{c0} as a function of the angle between the applied field and the c axis of the crystal. (a) Data for the unirradiated region of the crystal in an applied field of 0.5 T and for a proton-irradiated crystal in applied fields of 1 and 4 T. (b) Data are shown for the region of the crystal irradiated with 1 GeV U ions in applied fields of 1 and 4 T and for a twinned crystal in a 4 T field. T^* was defined as the temperature where $\rho=1$ $\mu\Omega$ cm.

E. Angular dependence of the resistivity

1. Unirradiated region

The behavior of the normalized resistivity is shown as a function of the angle of the applied magnetic field with respect to the c axis of the crystal for $H=1$ T in Fig. 9. The magnetic field was tilted from 90° ($\|$ to the ab plane) to 0° ($\|$ c axis) for $T=92.4$ and 90.7 K. In twinned crystals, there is a sharp dip in the resistivity as H becomes aligned with the twin boundaries at $\theta=0°$.[7,69,70] In our crystal, the resistivity is a smooth function of the angle, which is typical for a clean, untwinned crystal. Note that the resistivity is largest when the field is aligned parallel with the c axis and is a maximum when the field is parallel with the ab plane. This angular dependence of the resistivity arises from the anisotropy of the material. In $YBa_2Cu_3O_{7-\delta}$, the mass anisotropy ratio ($m_c/m_{ab}=\gamma^2$) lies in the range of 25–100 (Ref. 52) [as discussed above we find $\gamma^2=(7.6)^2$ in our crystal].

2. Irradiated region

The angular dependence of the resistivity in the irradiated region of the crystal shows a dramatically different behavior as shown in Fig. 10(b). The data were obtained by applying

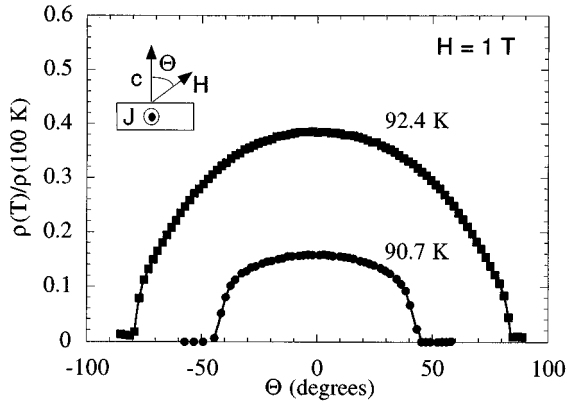

FIG. 9. Normalized resistivity as a function of the angle between the applied 1 T magnetic field and the c axis of the crystal for two different temperatures. The applied field was always perpendicular to the current.

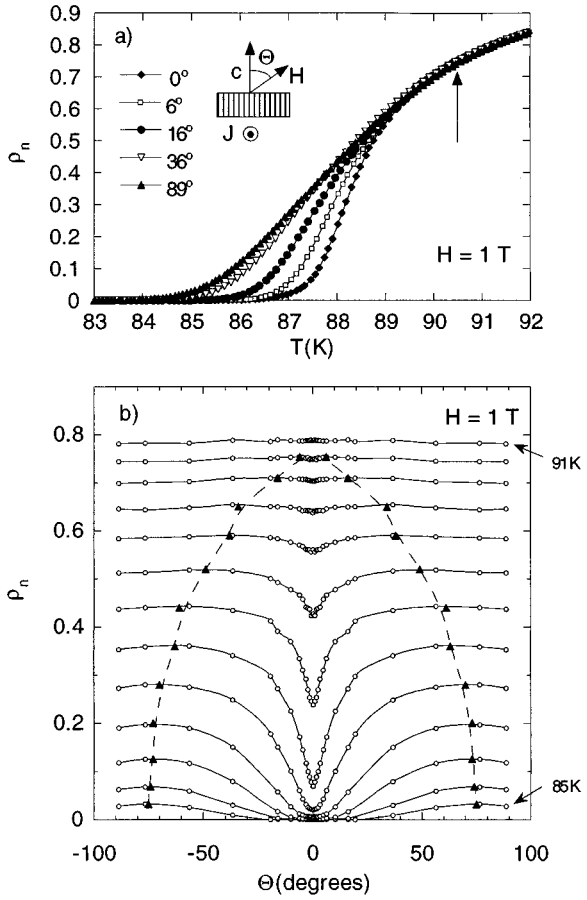

FIG. 10. (a) Normalized resistivity as a function of temperature for a 1 T field applied at various angles with respect to the c axis. The onset of pinning is indicated by the arrow. The field was always perpendicular to the current. (b) Normalized resistivity as a function of the angle between the applied field and the c axis of the crystal for temperatures between 85 and 91 K in 0.5 K intervals. The depinning angle at different temperatures is shown in (b) by the solid triangles. The solid and dashed lines are a guide to the eye.

a 1 T magnetic field at selected angles with respect to the c axis and then measuring the resistivity as a function of temperature at each angle as illustrated in Fig. 10(a). In Fig. 10(a) we show $\rho(T)/\rho(100\ \mathrm{K})$ in a 1 T field applied at $\Theta = -19.4°$, 0°, 0.8°, 1.5°, 2.3°, 3.2°, 4.7°, 6.2°, 10.1°, 16.0°, 36.6°, 56.3°, 76.5°, and 86.4° with respect to the crystallographic c axis of the crystal. Figure 10(b) was compiled by extracting the value of the normalized resistivity $\rho_n(\Theta)$ [where $\rho_n = \rho(T)/\rho(100\ \mathrm{K})$] at fixed temperatures from 85 to 91 K in 0.5 K increments. Since $\rho_n(\Theta)$ is symmetric about 0° we set $\rho(-\Theta) = \rho_n(\Theta)$ in Fig. 10(b).

In contrast to the unirradiated region of the crystal, the resistivity in the irradiated region of the crystal shows a pronounced dip near $\Theta = 0°$ for $T \leqslant 90.5$ K. This dip arises from the enhanced pinning of the vortices as they become aligned with the columnar defects which are parallel to the c axis. One remarkable feature of the $\rho_n(\Theta)$ curves is that the dip in the resistivity occurs even for temperatures in the fluctuation regime, i.e., for temperatures above the midpoint of the superconducting transition. The onset of this dip occurs at $T/T_{c0} \approx 1$ and very close to $\rho_n \approx 0.75$. We can compare these results to those found for single crystals irradiated with Xe and Au ion irradiation with $B_\phi = 2$ T,[71] where the onset of pinning occurred at $\rho_n = 0.17$ (Xe ions) and $\rho_n = 0.28$ (Au ions), respectively. This is one indication that the columnar defects created by U ion irradiation are highly effective pinners up to very high temperatures. These results also indicate that the strength of the pinning increases with the size of the ion used for the irradiation.

Another extraordinary feature of U ion irradiation is the strength of the columnar defect pinning at large angles. This is seen in the shape of the $\rho_n(\Theta)$ curves where $\rho_n(\Theta)$ first increases with decreasing Θ (similar to the unirradiated region of the crystal), and then begins decreasing as sections of the vortices become pinned by the columnar defects. We can define the depinning angle Θ_{depin} as half the angular distance between the maxima in $\rho_n(\Theta)$. The value of the depinning angle is shown in Fig. 10(b) by the solid triangles, the dashed line is a guide to the eye.

The depinning angle is shown as a function of temperature for $H = 1$ and 4 T in Fig. 11. These fields correspond to $B_\phi/2$ and $2B_\phi$, where $B_\phi = 2$ T is the matching field for this crystal. In both applied fields, the depinning angle increases roughly linearly with decreasing temperature near T_{c0} and then saturates to a maximum value at lower temperatures. In a 1 T applied field, this saturation value is ~75° and in 4 T the value is ~24°.

Doyle *et al.* reported the effects of 2.7-GeV U ion irradiation on $YBa_2Cu_3O_{7-\delta}$ thin films with $B_\phi = 0.4$ T.[37] They determined $J_c(\Theta)$ from magnetic measurements and found that the irradiated film showed an enhanced J_c up to angles of ~50° in a 1 T applied field at a reduced temperature $T/T_{c0} = 0.86$. This value is considerably below the value we found from the resistive measurements, most likely because of the lower matching field and possibly because of competing effects of the preexisting correlated defects in the film.

We can also compare our saturation values to those reported by Fleshler *et al.*[47] for twin boundary pinning. They reported values of ~25° in 1 T and ~20° in 4 T and a linear decrease of $\Theta_{\mathrm{depin}}(H)$ with a slope of $-1.6°/\mathrm{T}$. In contrast, we find a change of 50° in going from 1 to 4 T, representing

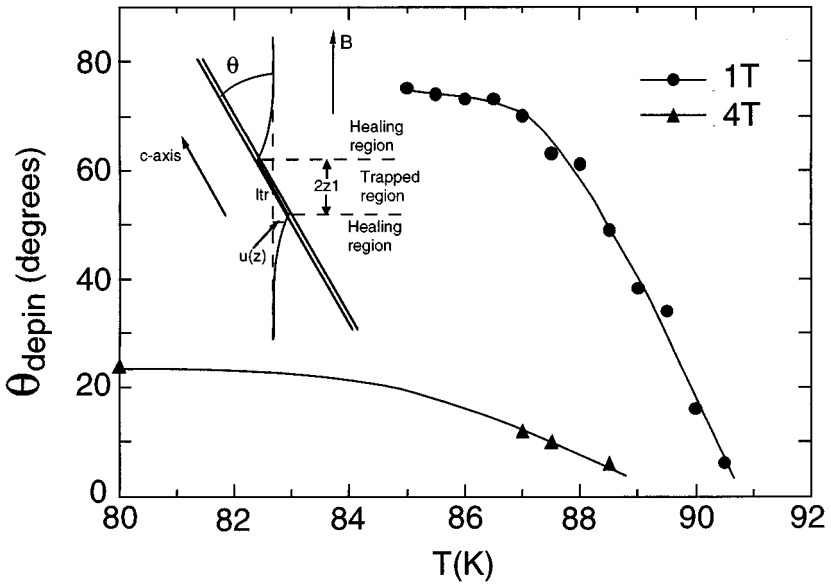

FIG. 11. Depinning angle as a function of reduced temperature for the irradiated region of the crystal measured in applied magnetic fields of 1 and 4 T. Solid lines are a guide to the eye. Inset shows the vortex pinning configuration in the presence of a columnar defect.

a slope which is roughly an order of magnitude larger ($-16.7°$/T).

The values of the depinning angles have been reported for $Tl_2Ba_2CaCu_2O_8$ films irradiated with Xe ions[24] and Ag ions.[15] In the Ag-irradiated films, the onset of pinning occurs at $T/T_{c0}\sim 0.85$ and the maximum value of $\Theta_{\rm depin}$ reported was $\sim 35°$ in an applied field of 1 T. For the Xe-irradiated film, the value of $\Theta_{\rm depin}$ was also $\sim 35°$ for $H=1$ T and $T=80$ K.[24] The smaller values for the onset temperature and $\Theta_{\rm depin}$ may be related to the smaller radius of the columnar defect and the greater anisotropy of $Tl_2Ba_2CaCu_2O_8$.

We can relate the observed angular depinning of the vortex system with the microscopic pinning characteristics. To this end let us first consider the angular behavior of the low-temperature pinning.[72] We estimate the strength of the pinning energy per unit length U_p from the depinning angle. When the field is applied at an angle Θ with respect to the columnar defect, a vortex line trapped in the columnar defect consists of three regions: a trapped piece of length $l_{\rm tr}=2z_1\cos\Theta$ and two ''healing'' regions (see inset to Fig. 11). Such a structure of pinned vortices was reported by Sonin for the case of twin boundary pinning.[73] Below we derive the expression for the energy of a pinned vortex in a simple way. The calculations are performed for the case of an isotropic superconductor. Generalization of the results for the anisotropic case is done using the scaling transformation.[74,75] The energy of the trapped region is given by

$$E_1=\int\left[\frac{\varepsilon_1}{2}\left(\frac{du}{dz}\right)^2+\frac{K}{2}u^2\right]dz-U_P l_{\rm tr}, \tag{3}$$

where $\varepsilon_1\approx[\Phi_0^2/(4\pi\lambda)^2]\ln(a_0/\xi)$ is a linear tension energy, $a_0\sim\sqrt{\Phi_0/B}$ is the distance between vortices, $(K/2)u^2$ represents the ''cage potential'' arising from the interaction with the other vortices, where $K=\Phi_0 B/(4\pi\lambda^2)$, and U_p is the pinning potential per unit length of the defect. The elastic approximation for the tilt energy is valid for tilting angles $\theta\ll 1$ for an isotropic superconductor which, according to the scaling rules,[74,75] corresponds to $\tan\theta\ll\gamma$ for the anisotropic case. Thus E_1 can be expressed as

$$E_1=2\left(U_P z_1+\frac{\varepsilon_1}{2}z_1\theta^2+\frac{Kz_1^3}{6}\theta^2\right). \tag{4}$$

In the healing region, the vortex displacement $u(z)$ obeys the equation

$$-\varepsilon_1\frac{d^2u}{dz^2}+Ku=0, \tag{5}$$

and therefore decreases exponentially as $z_1\Theta\exp(-k_0 z)$ where $k_0=\sqrt{K/\varepsilon_1}$. The energy of the two healing regions is given by

$$E_2=2\int dz\ K(z_1\theta)^2\exp(-2k_0 z)=\sqrt{K\varepsilon_1}(z_1\theta)^2, \tag{6}$$

so the total energy gain of the pinned vortex $E_{pv}=E_1+E_2$ is given by

$$E_{pv}=-2U_P z_1+\frac{\varepsilon_1^{3/2}\theta^2}{\sqrt{K}}\frac{(k_0 z_1+1)^3-1}{3} \tag{7}$$

and minimizing with respect to z_1 gives

$$k_0 z_1=\sqrt{\frac{2U_P}{\varepsilon_1\theta^2}}-1. \tag{8}$$

Therefore at low temperatures, where thermal energies can be neglected, the depinning angle coincides with the accommodation angle, where the accommodation angle is the angle at which the trapped length goes to zero:[52]

$$\theta_{\rm acc}=\sqrt{\frac{2U_P}{\epsilon_1}}. \tag{9a}$$

If the angle θ is not small, we can replace $\theta_{\rm acc}$ with $\tan\theta_{\rm acc}$. The general anisotropic result following from Eq. (9a) and from scaling arguments can be written as

TABLE I. Pinning energy per unit length calculated from the depinning angle using Eqs. (9b) and (11) for the U irradiated region of the crystal and for the twinned crystal.

Sample	Applied field $H(T)$	U_p (K/cm) From Eq. (11)	U_p (K/cm) From Eq. (9b)
U ion irradiated	1	2×10^8	1×10^8
U ion irradiated	4	5×10^7	
Twinned	1	5×10^7	
Twinned	4	4×10^7	

$$\tan\theta_{\rm acc}=\sqrt{\frac{2U_P}{\tilde{\varepsilon}_1}}, \tag{9b}$$

where $\tilde{\varepsilon}_1\approx[\Phi_0^2/(4\pi\lambda_c)^2]\ln(a_0/\xi)$ is the linear tension of the vortex line in an *anisotropic* superconductor. Using the expression for z_1 from Eq. (8), and the scaling transformation[74] we can write the energy of the pinned vortex in an anisotropic superconductor as

$$E_{pv}=\frac{2\tilde{\varepsilon}_1^{3/2}}{3\sqrt{K}}(\tan\theta_{\rm acc}-\tan\theta)^2\left(\frac{\tan\theta_{\rm acc}}{\tan\theta}+\frac{1}{2}\right). \tag{10}$$

Thermal fluctuations become important when k_BT becomes of order E_{pv}. At angles $\theta\leqslant\theta_{\rm acc}$, where the characteristic trapped length is of the order of a_0/γ, $E_{pv}\sim U_pa_0/\gamma$. At $k_BT<U_pa_0/\gamma$, the depinning angle $\theta_{\rm depin}$ is very close to the accommodation angle (9b). At higher temperatures when $k_BT>U_pa_0/\gamma$, the depinning angle is determined by thermal fluctuations and can be estimated by setting E_{pv} equal to k_BT. Thus we can find U_p from the depinning angle:

$$U_P\approx\varepsilon_0\left[\frac{2k_BT\tan\theta_{\rm depin}}{\varepsilon_0a_0}\right]^{2/3}. \tag{11}$$

In these equations, k_B is the Boltzman constant, $\Phi_0=2.1\times10^{-7}G$ cm^2 is the flux quantum, B is the applied magnetic field, and $\varepsilon_0\approx\Phi_0^2/(4\pi\lambda_{ab})^2$. In our calculations we assumed the temperature-dependent penetration depth was $\lambda_{ab}=1400\ \text{Å}/\sqrt{2(1-T/T_{c0})}$ and $\lambda_c=\gamma\lambda_{ab}$.

Table I shows the results of these calculations where we estimate U_p at $T/T_c=0.97$ for both the U-irradiated crystal and a twinned crystal in applied fields of 1 and 4 T. For the U-irradiated region in an applied field of $H=1$ T, we should calculate U_p using Eq. (9b) instead of Eq. (11) since $k_BT<U_pa_0/\gamma=120$ K. This yields $U_p\approx1\times10^8$, which is less than the value derived from Eq. (11). The reason that we get the same order of magnitude whether we use Eq. (9b) or Eq. (11) may be that at $T/T_c=0.87$ we are in the region where $\Theta_{\rm depin}$ is approaching $\Theta_{\rm acc}$. This is consistent with the temperature dependence of $\Theta_{\rm depin}$ for $H=1$ T seen in Fig. 11. The value of $\Theta_{\rm depin}$ begins to saturate at temperatures below $\sim$87 K, indicating a crossover from the depinning angle to the accommodation angle.

For the 1 T applied field, the pinning energy per unit length (from Eq. 9b) is approximately a factor of 2 higher in the U-irradiated crystal than in the twinned crystal. For the 4 T applied field, U_P is only $\sim$25% greater for the U ion irradiated crystal. The values of U_P drop with increasing field for both samples, but the rate of decrease in U_P is about two times larger for the U ion irradiated crystal. The larger field dependence of the U ion irradiated sample may be related to the applied field crossing over from one half the matching field to twice the matching field in going from 1 to 4 T. Our results are of the same order of magnitude reported by Dorosinskii *et al.* for twinned crystals. They report a value of $U_P\approx10^7$ K/cm for $t\sim0.92$ from low field, magneto-optical experiments.[76]

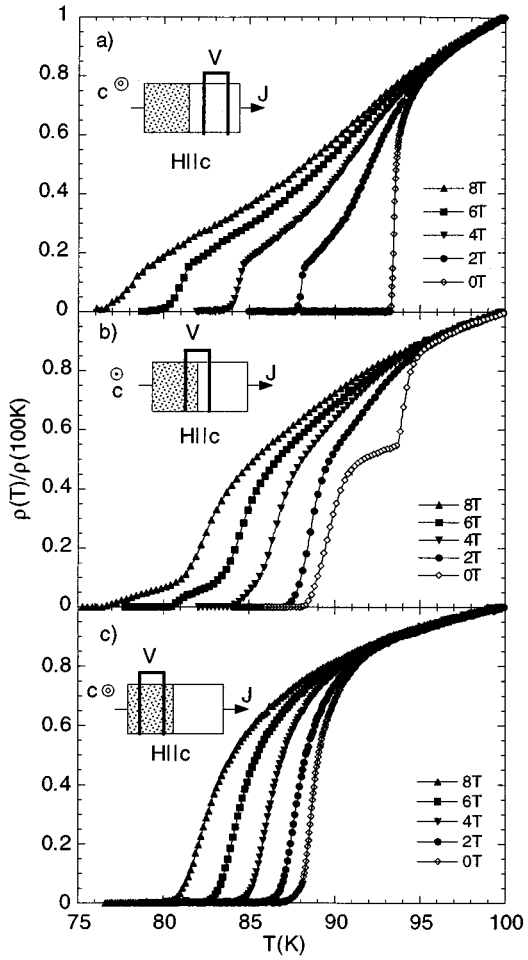

FIG. 12. Normalized resistivity as a function of temperature in fields from 0 to 8 T for $H\|c$ for three different regions of the crystal: (a) unirradiated region, (b) across the interface of the irradiated and unirradiated regions, and (c) the irradiated region. In all three cases, $J=0.7$ A/cm^2.

F. Resistive properties across both irradiated and unirradiated regions

Our unique irradiation geometry, which results in adjacent damaged and undamaged regions, allows the measurement of the vortex behavior in a composite region containing parts of both regions. Figure 12 shows the normalized resistivity as a function of temperature when $H\|c$ measured (a) across the unirradiated region, (b) across a composite region, and (c) across the irradiated region. These results show that the two regions of the crystal act like resistors in series. For example, for the $H=0$ T data, the superconducting transition

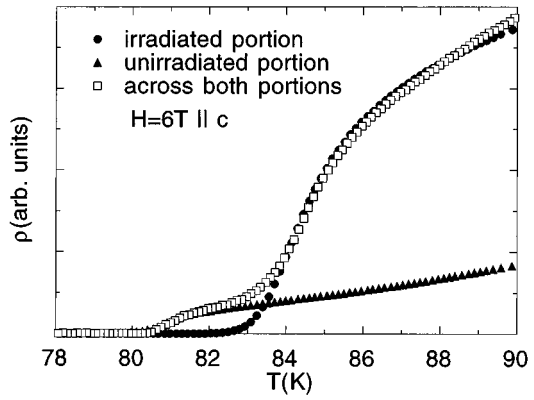

FIG. 13. Rescaled resistivity as a function of temperature as measured across the irradiated region (solid circles), the unirradiated region (solid triangles), and across both regions (open squares).

of each region is clearly reflected by the two sharp drops in resistivity in (b) measured across the composite.

This ''series'' behavior is seen clearly in Fig. 13, where we plot the normalized resistivity for each region on the same plot. In order to highlight the salient features of the curves, we rescaled the magnitude of the normalized resistivity of each region so the curves would lie on top of each other. (The scaling factors were 0.2 for the unirradiated region, 0.6 for the unirradiated region and 1 for the interface region.) The resistivity measured across both regions clearly displays a double transition, associated with the irradiated and unirradiated regions in the sample.

IV. CONCLUSIONS

The effect of columnar defects induced by uranium heavy ion irradiation has been investigated in a twin-free crystal of $YBa_2Cu_3O_{7-\delta}$. The quality of this crystal is indicated by the observation of a sharp ''kink'' in the temperature dependence of the resistivity associated with the first-order vortex liquid to solid phase transition. We used a mask during the irradiation of the twin-free crystal to fabricate a composite sample where one part was nearly defect free and the other part was populated with columnar defects induced by 1-GeV uranium ion irradiation. This unique geometry enabled us to study the effect of vortex pinning due to columnar defects, while at the same time preserving the preirradiation characteristics in part of the crystal. Furthermore, it enabled us to study the vortex dissipation properties across a combination of the columnar pinned region and relatively defect free, unpinned region, and directly demonstrate the dual nature of the dissipation.

Irradiation of the twin-free crystal completely suppresses the first-order vortex melting transition and shifts the irreversibility line near T_{c0} to higher fields. More remarkably, we see a reversal in the anisotropy of the irreversibility lines for $H\|c$ and $H\|ab$, implying that the U irradiation-induced columnar defects are strong enough to reverse the inherent pinning anisotropy of the crystal. Furthermore, the onset of pinning in the uranium ion irradiated region appears at very high temperatures ($T\approx T_{c0}$, the zero-field transition temperature), well into the superconducting fluctuation regime of the vortex liquid state. This is unlike the situation seen for irradiation with lighter ions like Au and Xe, where the onset of pinning occurs at much lower temperatures. The increase in the temperature of the onset of pinning suggests that the size of the columnar defects has a dramatic influence on the pinning. This dependence may be related to a matching effect between the radius of the vortex core (which is defined by the temperature-dependent coherence length) and the diameter of the columnar defect.

While we do not find the expected scaling of the resistivity for a Bose glass in the irradiated region of the crystal, we do find the predicted cusp in the irreversibility line as a function of angle. The width of this cusp is larger than the values found in twinned crystals and is comparable to values reported[77] for crystals with splayed 1-GeV Xe ion irradiation, again emphasizing the strong pinning ability of the uranium-induced columnar defects.

Using a model which incorporates the vortex elasticity, vortex-vortex interaction, and the pinning energy, and taking into account the larger thermal energies, we obtain the pinning energy per unit length U_p from the value of the depinning angles and find that U_p is larger and shows a stronger field dependence in the U ion irradiated sample than in twinned crystals.

ACKNOWLEDGMENTS

This work was supported by the U.S. Department of Energy through the Faculty Research Participation Program administered by the Argonne Division of Educational Programs (LMP), by the National Science Foundation, Office of Science and Technology Centers under Contract No. DMR91-20000 (J.A.F., A.E.K.) and the U.S. Department of Energy, BES, Materials Science under Contract No. W-31-109-ENG-38 (W.K.K., V.M.V., G.W.C., B.G.G.).

*Present address: 313 Microelectronics, 208 N. Wright Street, University of Illinois, Urbana, IL 61801.

[1] E. Zeldov, D. Majer, M. Konczykowski, V. B. Geshkenbein, V. M. Vinokur, and H. Shtrikman, Nature (London) **375**, 373 (1995).

[2] P. L. Gammel, L. F. Schneemeyer, J. V. Waszczak, and D. J. Bishop, Phys. Rev. Lett. **61**, 1666 (1988)

[3] H. Pastoriza, M. F. Goffman, A. Arribere, and F. d. l. Cruz, Phys. Rev. Lett. **72**, 2951 (1994).

[4] T. Hanaguri, T. Tsuboi, A. Maeda, T. Nishizaki, N. Kobayashi, Y. Kotaka, J. Shimoyama, and K. Kishio, Physica C **256**, 111 (1996).

[5] M. Charalambous, J. Chaussy, P. Lejay, and V. Vinokur, Phys. Rev. Lett. **71**, 436 (1993).

[6] H. Safar, P. L. Gammel, D. A. Huse, D. J. Bishop, J. P. Rice, and D. M. Ginsberg, Phys. Rev. Lett. **69**, 824 (1992).

[7] W. K. Kwok, S. Fleshler, U. Welp, V. M. Vinokur, J. Downey, and G. W. Crabtree, Phys. Rev. Lett. **69**, 3370 (1992).

[8] J. A. Fendrich, U. Welp, W. K. Kwok, A. E. Koshelev, G. W. Crabtree, and B. W. Veal, Phys. Rev. Lett. **77**, 2073 (1996).

[9] U. Welp, J. A. Fendrich, W. K. Kwok, G. W. Crabtree, and B. Veal, Phys. Rev. Lett. **76**, 4809 (1995).

[10] A. Schilling, R. A. Fisher, N. E. Phillips, U. Welp, D. Dasgupta,

W. K. Kwok, and G. W. Crabtree, Nature (London) **382**, 791 (1996).
[11] L. Ruixing, D. A. Bonn, and W. N. Hardy, Phys. Rev. Lett. **76**, 835 (1996).
[12] J. A. Fendrich, W. K. Kwok, J. Giapintzakis, C. J. van der Beek, V. M. Vinokur, S. Fleshler, U. Welp, H. K. Viswanathan, and G. W. Crabtree, Phys. Rev. Lett. **74**, 1210 (1995).
[13] R. H. Koch, V. Foglietti, W. J. Gallagher, F. Koren, A. Gupta, and M. P. A. Fisher, Phys. Rev. Lett. **63**, 1511 (1989).
[14] W. Jiang, N.-C. Yeh, D. S. Reed, U. Kriplani, D. A. Beam, M. Konczykowski, T. A. Tombrello, and F. Holtzberg, Phys. Rev. Lett. **72**, 550 (1994).
[15] R. C. Budhani, W. L. Holstein, and M. Suenaga, Phys. Rev. Lett. **72**, 566 (1994).
[16] L. Krusin-Elbaum, L. Civale, G. Blatter, A. D. Marwick, F. Holtzberg, and C. Feild, Phys. Rev. Lett. **72**, 1914 (1994).
[17] D. S. Reed, N.-C. Yeh, M. Konczykowski, A. V. Samoilov, and F. Holtzberg, Phys. Rev. B **51**, 16 448 (1995).
[18] C. A. Murray, P. L. Gammel, D. J. Gammel, D. B. Mitzi, and A. Kapitulnik, Phys. Rev. Lett. **64**, 2312 (1990).
[19] T. K. Worthington, E. Olsson, C. S. Nichols, T. M. Shaw, and D. R. Clarke, Phys. Rev. B **43**, 10 538 (1991).
[20] M. P. A. Fisher, Phys. Rev. Lett. **62**, 1415 (1989).
[21] D. R. Nelson, and V. M. Vinokur, Phys. Rev. Lett. **68**, 2398 (1992).
[22] D. R. Nelson, and V. M. Vinokur, Phys. Rev. B **48**, 13 060 (1993).
[23] M. Leghissa, T. Schuster, W. Gerhauser, S. Klaumunzer, M. R. Koblischka, H. Kronmuller, H. Kuhn, H.-W. Neumuller, and G. Saemann-Ischenko, Europhys. Lett. **19**, 323 (1992).
[24] K. E. Gray, J. D. Hettinger, D. J. Miller, B. R. Washburn, C. Moreau, C. Lee, B. G. Glagola, and M. M. Eddy, Phys. Rev. B **54**, 3622 (1996).
[25] C. J. van der Beek, M. Konczykowski, V. M. Vinokur, T. W. Li, P. H. Kes, and G. W. Crabtree, Phys. Rev. Lett. **74**, 1214 (1994).
[26] D. Bourgault, S. Bouffard, M. Toulemonde, D. Groult, J. Provost, F. Studer, N. Nguyen, and B. Raveau, Phys. Rev. B **39**, 6549 (1989).
[27] B. Hensel, B. Roas, S. Henke, R. Hopgengartner, M. Lippert, J. P. Strobel, M. Vildic, and G. Saemann-Ischenko, Phys. Rev. B **42**, 4135 (1990).
[28] M. Konczykowski, F. Rullier-Albenque, E. R. Yacoby, A. Shaulov, Y. Yeshurun, and P. Lejay, Phys. Rev. B **44**, 7167 (1991).
[29] J. R. Thompson, Y. R. Sun, H. R. Kerchner, K. K. Christen, B. C. Sales, B. C. Chakoumakos, A. D. Marwick, and L. Civale, Appl. Phys. Lett. **60**, 2306 (1992).
[30] R. C. Budhani, M. Suenaga, and S. H. Liou, Phys. Rev. Lett. **69**, 3816 (1992).
[31] A. D. Marwick, L. Civale, L. Krusin-Elbaum, R. Wheeler, J. R. Thompson, T. K. Worthington, M. A. Kirk, Y. R. Sun, H. R. Kerchner, and F. Holtzberg, Nucl. Instrum. Methods Phys. Res. B **80-81**, 1143 (1993).
[32] T. Ishida, K. Okuda, Y. Kazumata, S. Okayasu, and O. Michikami, Physica C **247**, 206 (1995).
[33] V. Hardy, C. Simon, J. Provost, and D. Groult, Physica C **206**, 220 (1993).
[34] L. Civale, A. D. Marwick, T. K. Worthington, M. A. Kirk, J. R. Thompson, L. Krusin-Elbaum, Y. Sun, J. R. Clem, and F. Holtzberg, Phys. Rev. Lett. **67**, 648 (1991).
[35] D. K. Christen, S. Zhu, C. E. Klabunde, H. R. Kerchner, J. R. Thompson, R. Feenstra, L. Civale, and J. M. Phillips, Physica B **194-196**, 1825 (1994).
[36] R. C. Budhani, Y. Zhu, and M. Suenaga, in *Superconductivity and Its Applications*, edited by H. S. Kwok, D. T. Shaw, and M. J. Naughton (AIP, Buffalo, 1992).
[37] R. A. Doyle, W. S. Seow, J. D. Johnson, A. M. Campbell, P. Berghuis, R. E. Somekh, J. E. Evetts, G. Wirth, and J. Wiesner, Phys. Rev. B **51**, 12 763 (1995).
[38] J. D. Hettinger, A. G. Swanson, W. J. Skocpol, J. S. Brooks, J. M. Graybeal, P. M. Mankiewich, R. E. Howard, B. L. Straughn, and E. G. Burkhardt, Phys. Rev. Lett. **62**, 2044 (1989).
[39] M. Konczykowski, F. Rullier-Albenque, Y. Yeshurun, E. R. Yacoby, A. Shaulov, and P. Lejay, Physica C **185-189**, 2347 (1991).
[40] L. Civale, G. Pasquini, P. Levy, G. Nieva, D. Casa, and H. Lanza, Physica C **263**, 389 (1996).
[41] E. R. Nowak, S. Anders, H. M. Jaeger, J. A. Fendrich, W. K. Kwok, R. Mogilevsky, and D. G. Hinks, Phys. Rev. B **54**, 12 725 (1996).
[42] H. Frank, J. Lethen, L. Buschmann, B. Decker, J. Wiesener, G. Wirth, P. Wagner, H. Adrian, P. Lemmens, and G. Güntherodt, Physica C **259**, 142 (1996).
[43] J.-Y. Lin, M. Gurvitch, S. K. Tolpygo, A. Bourdillon, S. Y. Hou, and J. M. Phillips, Phys. Rev. B **54**, R12 717 (1996).
[44] K. Harada, H. Kasai, O. Kamimura, T. Matsuda, A. Tonomura, S. Olayasu, and Y. Katzumata, Phys. Rev. B **53**, 9400 (1996).
[45] D. L. Kaiser, F. Holtzberg, M. F. Chisholm, and T. K. Worthington, J. Cryst. Growth **85**, 593 (1987).
[46] J. P. Biersack, and J. F. Ziegler, Transport of Ions in Matter (TRIM)-Monte Carlo Simulation Program, Ver. 91.14.
[47] S. Fleshler, W. K. Kwok, U. Welp, V. M. Vinokur, M. K. Smith, J. Downey, and G. W. Crabtree, Phys. Rev. B **47**, 14 448 (1993).
[48] W. K. Kwok, U. Welp, V. M. Vinokur, S. Fleshler, J. Downey, and G. W. Crabtree, Phys. Rev. Lett. **67**, 390 (1991).
[49] W. N. Kang, D. H. Kim, S. Y. Shim, J. H. Park, T. S. Hahn, S. S. Choi, W. C. Lee, J. D. Hettinger, K. E. Gray, and B. Glagola, Phys. Rev. Lett. **76**, 16 (1996).
[50] U. Welp, S. Fleshler, W. K. Kwok, R. A. Klemm, V. M. Vinokur, J. Downey, B. Veal, and G. W. Crabtree, Phys. Rev. Lett. **67**, 3180 (1991).
[51] R. Ikeda, T. Ohmi, and T. Tsuneto, J. Phys. Soc. Jpn. **60**, 1051 (1991).
[52] G. Blatter, M. V. Feigel'man, V. B. Geshkenbein, A. I. Larkin, and V. M. Vinokur, Rev. Mod. Phys. **66**, 1125 (1994).
[53] C. J. Lobb, Phys. Rev. B **36**, 3930 (1987).
[54] H. Safar, P. L. Gammel, D. A. Huse, D. J. Bishop, W. C. Lee, J. Giapintzakis, and D. M. Ginsberg, Phys. Rev. Lett. **70**, 3800 (1993).
[55] N.-C. Yeh, Phys. Rev. B **40**, 4566 (1989).
[56] A. Houghton, R. A. Pelcovits, and A. Sudbo, Phys. Rev. B **40**, 6763 (1989).
[57] L. Krusin-Elbaum, L. Civale, F. Holtzberg, A. P. Malozemoff, and C. Feild, Phys. Rev. Lett. **67**, 3156 (1991).
[58] A. Schilling, H. R. Ott, and T. Wolf, Phys. Rev. B **46**, 14 253 (1992).
[59] D. E. Farrell, J. P. Rice, and D. M. Ginsberg, Phys. Rev. Lett. **67**, 1165 (1991).
[60] A. Umezawa, G. W. Crabtree, J. Z. Liu, T. J. Moran, S. K. Malik, L. H. Nunez, W. K. Kwok, and C. H. Sowers, Phys. Rev. B **38**, 2843 (1988).
[61] D. E. Farrell, J. P. Rice, D. M. Ginsberg, and J. Z. Liu, Phys. Rev. Lett. **64**, 1573 (1990).
[62] U. Welp, W. K. Kwok, G. W. Crabtree, K. G. Vandervoort, and J.

Z. Liu, Phys. Rev. Lett. **62**, 1908 (1989).
[63] D. E. Farrell, C. M. Williams, S. A. Wolf, N. P. Bansal, and V. G. Kogan, Phys. Rev. Lett. **61**, 2805 (1988).
[64] L. Krusin-Elbaum, R. L. Greene, F. Holtzberg, A. P. Malozemoff, and Y. Yeshurn, Phys. Rev. Lett. **62**, 217 (1989).
[65] R. G. Beck, D. E. Farrell, J. P. Rice, D. M. Ginsberg, and V. G. Kogan, Phys. Rev. Lett. **68**, 1594 (1992).
[66] T. T. M. Palstra, B. Batlogg, R. B. v. Dover, L. F. Schneemeyer, and J. V. Waszczak, Phys. Rev. B **41**, 6621 (1990).
[67] C. Simon, J. Provost, D. Groult, V. Hardy, A. Wahl, C. Goupil, and A. Ruyter, Nucl. Instrum. Methods Phys. Res. B **107**, 384 (1996).
[68] L. M. Paulius, A. M. Petrean, W.-K. Kwok, and J. A. Fendrich (unpublished).
[69] W.-K. Kwok, U. Welp, V. M. Vinokur, S. Fleshler, J. Downey, and G. Crabtree, Phys. Rev. Lett. **67**, 390 (1991).
[70] E. M. Gyorgy, R. B. van Dover, L. F. Schneemeyer, A. E. White, H. M. O'Bryan, R. J. Felder, J. V. Waszczak, and W. W. Rhodes, Appl. Phys. Lett. **56**, 2465 (1990).
[71] D. Dasgupta, J. A. Fendrich, W.-K. Kwok, and G. W. Crabtree, Bull. Am. Phys. Soc. **41**, 712 (1996).
[72] L. Burlachkov, V. B. Geshkenbein, A. E. Koshelev, and V. M. Vinokur (unpublished).
[73] E. B. Sonin, Phys. Rev. B **48**, 10 287 (1993).
[74] R. A. Klemm, and J. R. Clem, Phys. Rev. B **21**, 1868 (1980).
[75] G. V. Blatter, V. B. Geshkenbein, and A. I. Larkin, Phys. Rev. Lett. **71**, 68 (1992).
[76] L. A. Dorosinskii, V. I. Nikitenko, A. A. Polyanskii, and V. K. Vlasko-Vlasov, Physica C **246**, 283 (1995).
[77] D. S. Reed, N.-C. Yeh, W. Jiang, U. Kriplani, M. Konczykowski, and F. Holtzberg, Int. J. Mod. Phys. B **10**, 2723 (1996).